Free Convective Heat Transfer in an Enclosure Filled with Porous media with and without Insulated Moving Wall

Laith Jaafer Habeeb

Mechanical Engineering Dept., University of Technology, Baghdad – Iraq (e-mail: laithjaafer@yahoo.com , or, dr.laith_jaafer@uotechnology.edu.iq).

ABSTRACT

The present work is concerned with the free convective two dimensional flow and heat transfer, in isotropic fluid filled porous rectangular enclosure with differentially heated walls for steady state incompressible flow have been investigated for non-Darcy flow model. Effects of Darcy number ($0.0001 \le Da \le 10$), Rayleigh number ($10 \le Ra \le 5000$), and aspect ratio ($0.25 \le AR \le 4$), for a range of porosity ($0.4 \le \varepsilon \le 0.9$) with and without moving lower wall have been studied. The cavity was insulated at the lower and upper surfaces. The right and left heated surfaces allows convective transport through the porous medium, generating a thermal stratification and flow circulations. It was found that the Darcy number, Rayleigh number, aspect ratio, and porosity considerably influenced characteristics of flow and heat transfer mechanisms. The results obtained are discussed in terms of the Nusselt number, vectors, contours, and isotherms.

Keywords: Numerical study, moving-wall cavity, porous medium, Darcy and Rayleigh numbers.

انتقال الحرارة بالحمل الحر في حيز مملوء بوسط مسامي مع وبدون تحريك جدار معزول

م.د. ليث جعفر حبيب – الجامعة التكنولوجية – قسم هندسة المكائن والمعدات

الخلاصة

ان العمل الحالي يبحث انتقال الحرارة والجريان للحمل الحر ثنائي البعد في مائع ذو خواص ثابتة في حيز مستطيل مملوء بمادة مسامية ذو جدران مسخنة بشكل مختلف وذلك للحالة الثابتة لجريان غير قابل للإنضغاط لنموذج جريان لا- دارسي. تم دراسة تأثير رقم دارسي ($0.0001 \le Da \le 10$) ورقم رايلي ($10 \le Ra \le 5000$) ونسبة العرض للإرتفاع ($0.25 \le AR \le 4$) لمدى نفاذية ($0.4 \le \varepsilon \le 0.9$) مع وبدون تحريك الجدار السفلي للحيز. لقد تم عزل السطحين العلوي والسفلي للتجويف. وان السطحين الايمن والايسر يسمحان لإنتقال الحمل خلال الوسط المسامي وينتج عن ذلك طبقات حرارية ودوامات جريان. لقد وجد بأن رقم دارسي ورقم رايلي ونسبة العرض للإرتفاع والمسامية هي عوامل تؤثر بشكل كبير على الجريان وميكانيكية انتقال حرارة. لقد تم مناقشة النتائج المستحصلة برسم اشكال لرقم نسلت ومتجهات وكونتورات ومستويات درجات حرارة.

Nomenclature

AR	Aspect ratio
c	Micro velocity vector
e	Discrete velocity
F	Total body force due to the presence of porous media
f_i	Discretized density distribution function
f_i^{eq}	Discretized equilibrium density distribution function

G	Boussinesq effect
g	Acceleration due to gravity
g_i	Discretized internal energy distribution function
g_i^{eq}	Discretized equilibrium internal energy distribution function
H	Characteristic length
j	Vertical direction opposite to that of gravity
K	Permeability
p	Pressure
T	Temperature
T_m	Average temperature
t	Time
U_{lid}	Moving lower wall velocity
u	Velocity vector
x	Position

Greek Symbols

β	Bulk coefficient
χ	Thermal diffusivity
Δt	Time step
ε	Porosity
ρ	Density
τ	Time relaxation
υ	Kinematic viscosity
υ_ε	Effective viscosity
ω	Weight coefficient

Non-dimensional Numbers

Nu	Nusselt number
Pr	Prandtl number
Ra	Rayleigh number
Da	Darcy number

I. INTRODUCTION

A basic understanding of fluid flow and heat transfer in a lid-driven cavity filled with saturated porous medium with buoyancy effect for steady state case is important in many areas such as solar power collector, nuclear energy systems, chemical processing equipment, coating and industrial processes, galvanizing and metal coating, float glass manufacturing, dynamics of lakes and large reservoirs, crystal growth, food processing and so on. Numerous investigations have been conducted in the past on lid-driven cavity flow and heat transfer considering various combinations of the imposed temperature gradients and cavity configurations. Such configurations can be idealized by the simple rectangular geometry with regular boundary conditions yielding a well-posed problem. The resulting flow however, is rather complex even when the flow is purely shear driven for the isothermal case without any temperature gradient. When a temperature gradient is imposed such that the shear driven and buoyancy effects are of comparable magnitude then the resulting flow falls under the convection regime and the interaction and coupling of these effects makes the analysis more complex. In recent years, the Lattice Boltzmann Method (LBM) has received considerable attention as an alternative approach for simulating wide range of fluid flow. Unlike other numerical methods, LBM predicts the evolution of particle distribution function and calculates the macroscopic variables by taking moment

to the distribution function. (Nithiarasu *et al* 1997) outlined a double-diffusive natural convection in a fluid saturated porous medium using the finite element method. A generalized porous medium model was used to study both Darcy and non-Darcy flow regimes in an axisymmetric cavity. Results indicated that the Darcy number should be a separate parameter to understand flow characteristics in non-Darcy regime. It was also observed that an increase in radius ratio leads to higher Nusselt and Sherwood numbers along the inner wall. (Hakan 2006) performed a numerical work to analyze combined convection heat transfer and fluid flow in a partially heated porous lid-driven enclosure. The top wall of enclosure moves from left to right with constant velocity and temperature. Heater with finite length was located on the fixed wall where its center of location changes along the walls. The results were shown that the best heat transfer was formed when the heater was located on the left vertical wall. (Hakan 2007) investigated numerically the natural convection heat transfer in a partially cooled and inclined rectangular enclosure filled with saturated porous medium. One of side wall has constant hot temperature and one adjacent wall is partially cooled while the remaining ones were adiabatic. It was found that inclination angle was the dominant parameter on heat transfer and fluid flow as well as aspect ratio. (Ayad 2008) studied numerically two–dimensional, steady natural convection in a rectangular cavity filled with a heat generating saturated porous medium for the case when the vertical walls of the cavity were isothermal and the horizontal walls were either adiabatic or cold. The thermal convection flow together with the uniform heat generating produces a highly stratified medium at high Rayleigh numbers. The change in the horizontal wall boundary condition from adiabatic to cold reduces (θ_{max}) also it was found that heat transfer increase with increasing Rayleigh number while it decrease with aspect ratio. (Wang 2009) studied the lid-driven rectangular cavity containing a porous Darcy–Brinkman medium. It was found that the porous medium effect decreases both the strength and the number of recirculating eddies, especially for deep cavities. (Mohd *et al* 2010) investigated fluid flow behavior through porous media in a lid-driven square cavity. The Brinkman-Forcheimer equation was coupled with the lattice Boltzmann formulation to predict the velocity field in the system. They found that the magnitude of velocity, strength of vortex and velocity boundary layer was significantly affected porosity of the media. The lattice Boltzmann simulation scheme was capable in prediction of fluid flow behavior through porous media. (Mohamed and Wael 2010) concerned with the mixed convection in a rectangular lid-driven cavity under the combined buoyancy effects of thermal and mass diffusion. Double-diffusive convective flow in a rectangular enclosure with moving upper surface is studied numerically. Both upper and lower surfaces are being insulated and impermeable. Constant different temperatures and concentration are imposed along the vertical walls of the enclosure. In addition, the predicted results for both local and average Nusselt and Sherwood numbers are presented and discussed for various parametric conditions. (MOHD 2010) applied (LBM) to predict the phenomenon of natural convection in a generalized isotropic porous media model filled in a square geometry by introducing a force term to the evolution equation and porosity to the density equilibrium distribution function. The model was used for simulation at ε equal to 0.4, 0.6 and 0.9. (Waheed *et al* 2011) investigated numerically the mixed convective heat transfer in a fluid-saturated porous medium using the generalized non-Darcy model. The flow governing parameters including the Darcy, Richardson and Péclet numbers, and the length-to-height aspect ratio were varied in the range $10^{-3} \leq Da \leq 10$, $0.1 \leq Ri \leq 10$, $1 \leq Pe \leq 10^3$ and $0.5 \leq AR \leq 4$ respectively while the Reynolds number was held constant at a value of $Re = 100$ for all computations. The results showed that all the flow governing parameters have strong influence on the flow pattern and heat distribution within the enclosure. (Prakash and Satyamurty 2011) investigated the free convective flow and heat transfer, in an anisotropic fluid filled porous rectangular enclosure using Brinkman extended non-Darcy flow model. The studies involve simultaneous consideration of hydrodynamic and thermal anisotropy. However, the magnitude of the change in average Nusselt number depends on the parameter *Da*, characterizing the Brinkman extended non-Darcy flow. (Antonio 2012) used lattice-Boltzmann equation method to simulate non-Darcy flow in porous media. 2-D in-line and staggered arrangements of uniform cylinders

have been considered. The results of a comprehensive computational evaluation were reported: the range of validity of Darcy-Forchheimer equation was investigated and correlations for macroscopic transport properties were presented. His investigation covered both no-slip and the slip-flow regimes. (Wenchao and Yueying 2012) built dimensionless mathematical models of one-dimensional flow in the semi-infinite long porous media with threshold pressure gradient for the two cases of constant flow rate and constant production pressure on the inner boundaries. Through formula deduction, it was found that the velocity of the moving boundary is proportional to the second derivative of the unknown pressure function with respect to the distance parameter on the moving boundary, which is very different from the classical heat-conduction Stefan problems. It was shown that for the case of constant flow rate the effect of the dimensionless threshold pressure gradient on the dimensionless pressure distributions and the transient dimensionless production pressure was not very obvious; in contrast, for the case of constant production pressure the effect on the dimensionless pressure distributions was more obvious especially at the larger dimensionless distance near the moving boundary; and for the case of constant production pressure, the smaller the dimensionless threshold pressure gradient was, the larger the dimensionless pressure is, and the further the pressure disturbance area reached.

From the available literature, the study of moving wall –such as lower wall- of an enclosure filled with porous medium with wide range of Darcy and Rayleigh numbers are limited. So, my concern in this work is to study the effects of Darcy number, Rayleigh number, and aspect ratio for a range of porosity with and without moving lower wall which are not covered in the previous works.

II. PROBLEM DEFINITION AND GOVERNING EQUATIONS

A. Physical Model

A schematic of the system in the present study is shown in **Figure 1**. The system consists of a square enclosure with sides of length H, filled with a fluid saturated porous medium and Prandlt number (Pr) =1.0. The problem has been studied assuming that the gravitational acceleration acts in the negative y-direction. As the square enclosure are long enough, so the flow is consider to be two dimensional, the fluid and the solid matrix are in thermal equilibrium, and the porous medium is homogeneous. This study will be limited to: steady state incompressible fluid flow, square enclosure with differentially heated walls, isotropic porous media, and non-Darcy region.

The directions of vortex rotation generated under the 84 different conditions were examined here. Always the left and right walls are subjected to hot and cold temperatures (non-dimensions 1.0 and 0.0) respectively, and the upper and lower walls are insulated (assumed to be adiabatic). The moving lid or wall is considered to be the lower one in this study, which is moved to the right ($+x$ direction).

In cases (1-18) -for this study- no wall movement is applied for Darcy number (Da = 0.0001, 0.001, 0.01, 0.1 1.0, and 10.0) each at porosity (ε = 0.4, 0.6, and 0.9) and Rayleigh number ($Ra = 10^4$).

In cases (19-36) the lower wall is moving at 0.2 m/s and for Darcy number (Da = 0.0001, 0.001, 0.01, 0.1 1.0, and 10.0) each at porosity (ε = 0.4, 0.6, and 0.9) and Rayleigh number ($Ra = 10^4$) to study the movement effect.

In cases (37-54) again no wall movement is considered for Rayleigh number (Ra = 10, 50, 100, 500, 1000, and 5000) each at porosity (ε = 0.4, 0.6, and 0.9) and Darcy number (Da = 0.01).

In cases (55-72) the lower wall is moving at 0.2 m/s and again for Rayleigh number (Ra = 10, 50, 100, 500, 1000, and 5000) each at porosity (ε = 0.4, 0.6, and 0.9) and Darcy number (Da = 0.01) to show the movement effect.

In cases (73-78), a stationary wall is required at (Ra = 1000), (Da = 0.01), and aspect ratio (AR = 0.25 and 4.0) each at porosity (ε = 0.4, 0.6, and 0.9) respectively.

In cases (79-84), a moving wall is required at (*Ra* = 1000), (*Da* = 0.01), and aspect ratio (*AR* = 0.25 and 4.0) each at porosity (ε = 0.4, 0.6, and 0.9) respectively to study the movement effect.

All these cases are studied in this paper, and only selected cases are mentioned for not to be extensive.

B. Materials and Methods

Following [6], [8], and [13] the generalized model for incompressible fluid flow through porous media can be expressed by the following equations:

$$\nabla \cdot u = 0 \tag{1}$$

$$\partial u/\partial t + (u \cdot \nabla)(u/\varepsilon) = -(1/\rho)\nabla(\varepsilon\, p) + \upsilon_{\varepsilon}\nabla^2 u + F \tag{2}$$

F represents the total body force due to the presence of porous media and is given by:

$$F = -(\varepsilon\upsilon/K)u - \left(1.75/\sqrt{150\varepsilon K}\right)|u|\, u + \varepsilon\, G \tag{3}$$

The permeability (*K*) of which can be related to no dimensional parameter of Darcy number *Da* as follow:

$$K = Da \times H^2 \tag{4}$$

In the formulation of LBM, the starting point is the evolution equation, discrete in space and time, for a set of distribution functions *f*. If a two-dimensional nine-velocity model (D2Q9) is used for flow field and two-dimensional four-speed (D2Q4) Lattice Boltzmann equation (LBE) model is used to simulate the temperature field, then the evolution equations for a given *f* and *g* takes the following forms:

$$f_i(x + e_i\Delta t, t + \Delta t) - f_i(x,t) = -1/\tau_f \left[f_i(x,t) - f_i^{eq}(x,t)\right] + F_i \tag{5}$$

$$g_i(x + e_i\Delta t, t + \Delta t) - g_i(x,t) = -1/\tau_g \left[g_i(x,t) - g_i^{eq}(x,t)\right] \tag{6}$$

Where $i = 0,1,\ldots,8$ for f and $i = 1,2,3,4$ for g.

Where distribution function f_i s used to calculate density and velocity fields while distribution function is used to g_i to calculate temperature field. Here, *e* denotes the discrete velocity set and expressed as:

$$e_i = \begin{cases} (0,0), & i = 0 \\ (\pm 1,0),(0,\pm 1), & i = 1\text{-}4 \\ (\pm 1,\pm 1), & i = 5\text{-}8 \end{cases} \tag{7}$$

f_i^{eq} , g_i^{eq} are equilibrium distribution functions, the choice of which determines the physics inherent in the simulation. For D2Q9 and (D2Q4) models, f_i^{eq} and g_i^{eq} are expressed as:

$$f_i^{eq} = \rho\omega_i\left[1 + 3e_i \cdot u + (9/2)\left((e_i \cdot u)^2/\varepsilon\right) - (3/2)\left((u)^2/\varepsilon\right)\right] \tag{8}$$

$$g_{1,2,3,4}^{eq} = \rho T(1/4)\left[1 + \left(e_i \cdot u / c^2\right)\right] \tag{9}$$

Where, the weights are ω_0= 4/9, $\omega_{1\text{-}4}$= 1/9 and $\omega_{5\text{-}8}$= 1/36. The time relaxation and the effective viscosity can be related as follow:

$$\upsilon_\varepsilon = (1/3)(\tau - (1/2)) \tag{10}$$

In order to obtain the correct macroscopic governing equations, the forcing term F_i must be expressed in terms of medium porosity as follow:

$$F_i = \rho\omega_i(1 - (1/2\tau)) \cdot \left[3e_i \cdot F + \left(9(uF : e_i e_i)^2/\varepsilon\right) - (3u \cdot F/\varepsilon)\right] \tag{11}$$

The macroscopic density and the macroscopic flow velocity can then be calculated as follow:

$$\rho = \sum_{i=1}^{9} f_i^{eq} \tag{12}$$

$$v = \sum_i e_i f_i / \rho + (\varepsilon G/2) \tag{13}$$

and:

$$u = v\Big/\left(c_0 + \sqrt{c_0^2 + c_1|v|}\right) \tag{14}$$

where:

$$c_0 = (1 + \varepsilon\upsilon/2K)\Big/2 \quad and \quad c_1 = 1.75\varepsilon\Big/2\sqrt{150\varepsilon^2 K}$$

It is noted that, if we set ε = 1, the Lattice Boltzmann equation reduces to the standard equation of free fluid flows.

Boussinesq approximation is applied to the buoyancy force term. With this approximation, it is assumed that all fluid properties are constant except for density change with temperature.

$$G = \beta g(T - T_m)j \tag{15}$$

The dynamical similarity depends on three dimensionless parameters: the Prandtl number (*Pr*), Rayleigh number (Ra) and Nusselt number (*Nu*).

$$Pr = \upsilon / \chi \tag{16}$$

$$Ra = \rho\beta(T_h - T_c)L^3 / \upsilon\chi \tag{17}$$

$$Nu = (H/\chi\Delta T)(1/H^2)\int_0^H\int_0^H q_x(x,y)dx\,dy \quad (18)$$

Where: $q_x(x,y) = uT - \chi(\partial/\partial x)T(x,y)$ is the local heat flux in *x*-direction.

III. NUMERICAL SIMULATION

The present algorithm used is the same in [8] and [13], it begin with main program with seven subroutines. The program is modified to fulfill the required different present cases and to handle more complex geometries. The numerical data obtained for each node are used to plot graphical representation of vectors, contours and isotherms. Simulations were done by programming which uses Fortran PowerStation 4.0 (Microsoft Developer Studio). Desktop PC with Intel (R) Core(TM)2 Quad CPU, 3 GHz processor and 4.00 GB RAM was used to run the simulation.

Numerical stability and iteration to converge need the particles to be at equilibrium state. This will be obtained by manipulating the value of the time relaxation. The value of time relaxation needs to be closer to 1 (1.1). The closer time relaxation to 1, the more number of particles will be exchanged to equilibrium state. The main iteration is repeated until a convergence solution is obtained at convergence criteria for the velocity less than 1×10^{-8}. In the simulations, mesh sizes (101×101), (201×51), and (51×201) were used for cases (1-72), (73-75 & 79-81), and (76-78 & 82-84) respectively.

The calculations of average Nusselt numbers for the present program are compared early by [8] or [13] with other single phase fluid results for different values of Rayleigh number and the present Lattice Boltzmann model for simulation of Brinkman-Forchheimer equation is verified. The comparison showed that the obtained Nusselt number is acceptable.

IV. RESULTS AND DISCUSSION

The results are presented for (84) different cases corresponding to *thirty six* Darcy-porosity effects, moreover to *thirty six* Rayleigh-porosity relationships and *twelve* aspect ratio-porosity arrangements all with and without moving wall. The best case of moving wall is when the lower wall is moving to the right and the maximum heat transfer occurs at 0.2 m/s as concluded in [13] for Ra = 1000, ε = 0.7, and Da = 0.01. Thus in this work at moving wall cases, the lower wall is moving to the right at 0.2 m/s. The basic features of flow and heat transfer are analyzed with the help of the vectors, contour patterns and isothermal contours. Also, average Nusselt numbers for all cases are tabulated and velocity components are plotted. Some of the results (that I find paper to compare with) have the same behavior of the similar published cases. Heat transfer in low speed lid-driven cavity flow is treated mostly as mixed convection. The flow driven by the movement of the wall is creating a forced convection conditions while temperature difference across the cavity causes a buoyancy driven, secondary flow. Thus, complicated patterns of heat and mass transfer occur inside the cavity.

A. Darcy Number and Movement Effect

Figure 2 shows the velocity vectors and temperature contours for the stationary wall for the square cavity filled with porous medium at Ra = 10^4 and thermal diffusivity (χ = 0.2) . **Figure 2-A** and **B** show the velocity vectors with *y*-component velocity contours and temperature contours respectively for Da = 0.0001 and ε = 0.4. The vectors form a clockwise unicellular circulating flow pattern. One big upper clockwise vortex is appeared because of the density effect due to heating. For the isotherms, it can be observed that they are mostly parallel to the vertical hot and cold walls indicating that

conductive heat transfer dominates. **Figure 2-C** predicts the velocity vectors with *y*-component velocity contours for $Da = 0.0001$ and $\varepsilon = 0.9$. Porosity does not seem to significantly affect the pattern only for the vortex center to be moved upward. **Figure 2-D** illustrates the temperature contours for $Da = 0.01$ and $\varepsilon = 0.6$. As the Darcy number and the porosity increase, there is a tendency of the lines to becoming less parallel. This is due to the fact that the inertial and non-linear drag terms are becoming less significant as the porosity increases, leading to higher dimensionless flow velocities which start to initiate convection. Also, at a lower Darcy number of 10^4, the velocity vectors (not shown here) are seen to violate the no-slip condition, with maximum magnitude near the wall. This is a typical characteristic of approximately Darcian flow regime. With increase in Darcy number 10^2, the flow satisfies the no-slip boundary condition on the walls. The point to be noted here is , the present generalized flow model predicts both the slip flow at lower Darcy numbers (near Darcian regime) and the no-slip flow condition at higher Darcy numbers (non-Darcian flow regime). **Figure 2-E** shows the velocity vectors with *y*-component velocity contours for $Da = 1.0$ and $\varepsilon = 0.4$. The elliptic shape of the vectors or of the vortex flow and the circular shape of the *y*-component velocity contours are now obvious. As the Darcy number and porosity increase, the circular shape vortex becomes more elliptic.

Figure 3 shows the temperature contours and velocity vectors for the lower wall movement for the square cavity filled with porous medium at $Ra = 10^4$ and thermal diffusivity ($\chi = 0.2$).

Figure 3-A, B, and **C** shows the temperature contours at $Da = 0.0001$ and $\varepsilon = 0.4$, 0.6, and 0.9 respectively. It is obvious that the lines are now mostly curvature. Convection dominates at this Rayleigh number condition and as the porosity increase; the curvature effect becomes stronger due to the fact that the inertial and non-linear drag terms are becoming less significant as the porosity increases, leading to higher dimensionless flow velocities which make convection more vigorous. However at areas near to the walls, heat conduction still dominates. The viscous effect from the walls retards the momentum of buoyancy force initiated by the differentially heated walls which slows down convective effect. The moving lid transfers the heat from the left side and the vortex caries the heat to the center. **Figure 3-D** predicts the velocity vectors at $Da = 0.01$ and $\varepsilon = 0.9$. When the lower wall moves to the right, two counterclockwise vortices are generated in the whole domain and a small clockwise vortex is generated near the left wall. **Figure 3-E** illustrates the temperature contours at $Da = 10.0$ and $\varepsilon = 0.9$. As it shown, the isotherms are distributed in whole domain resulting high Nusselt number.

Figure 4 shows the relationship between the average Nusselt number and Darcy number with and without movement at various porosities. When the Darcy number increases, the average Nusselt number is increases. But a significant increase in the average Nusselt number is detected at Darcy number range (0.0001-0.01) after that a small increase is noticed. As porosity increases, the average Nusselt number increases. A large increase in average Nusselt number is obtained when the lower wall is moved.

B. Rayleigh Number and Movement Effect

Figure 5 shows the velocities distributions (u) or *x*-component along the box *height* and (v) or *y*-component along the box *width* for $Da = 0.01$ with and without movement. Velocity components are plotted at mid width of the cavity and mid-height of the cavity respectively at different Rayleigh number and porosity. **Figure 5-A** shows the velocity distributions (*x*-component) for Ra = 10, 50, and 100 and $\varepsilon = 0.4$, 0.6, and 0.9 without movement. At the top of the cavity, a significant increase in *x*-component velocity as Rayleigh number and porosity are increase. **Figure 5-B** shows the velocity distributions (*y*-component) for Ra = 500, 1000, and 5000 and the same porosity range without movement. A significant increase in *y*-component velocity as Rayleigh number and porosity are

increase in the left hand side (+ values) and R.H.S. (- values). **Figure 5-C** shows the *x*-component velocity for Ra = 10 and ε = 0.4, 0.6, and 0.9 with movement. The velocity of the flow is higher near the hot vertical wall and it decreases continually with an increase in the horizontal distance. **Figure 5-D** shows the *y*-component velocity for Ra = 10 again at the same porosity range. The velocity of the flow is higher at the upper half of the cavity than that of bottom half. In the moving wall cases, a small increase in the velocity components due to *Ra* increase because of the high velocity magnitude of the moving wall comparing with the velocities of natural convection without movement.

C. Aspect ratio and movement effect

Figure 6 depicts the velocity vector with *y*-component velocity contours and temperature contour for *AR* = 0.25 and 4.0 at *Ra* = 1000 and *Da* = 0.01 with and without lower wall-driven. **Figure 6-A** and **B** show the velocity vectors with *y*-component velocity contours and temperature contours respectively at *AR* = 0.25 and ε = 0.4 without movement. One big clockwise vortex is appeared in the middle of the cavity approximately. The isotherms are being curvature near the hot wall and become vertical wherever it gets closer to the cold wall**. Figure 6-C** illustrates temperature contours at *AR* = 0.25 and ε = 0.9 again without movement. More curvature isotherms are being observed with higher temperatures near the hot wall. **Figure 6-D, E,** and **F** shows velocity vectors with *y*-component velocity contours at *AR* = 0.25 and ε = 0.4, 0.6, and 0.9 respectively with lower wall-driven. When porosity increases, movement would be spread well and vortex is formed to transfer fluid and heat. **Figure 6-G** and **H** shows velocity vectors and *y*-component velocity contours at *AR* = 4.0 and ε = 0.6 without movement. For a deep cavities there exists a string of eddies of rapidly decreasing strength. Note that the strengths of the deep eddies are very small, thus has little effect on the transport properties of the cavity. **Figure 6-I** and **J** illustrates velocity vectors and *y*-component velocity contours at *AR* = 4.0 and ε = 0.9 with lower wall-driven. More relevant is the dominant eddy adjacent to the moving lid.

Figure 7 shows the velocities distributions (*u*) or *x*-component along the box *height* and (*v*) or *y*-component along the box *width* for *AR* = 0.25 and 4.0 at *Ra* = 1000 and *Da* = 0.01 with and without lower wall-driven. Velocity components are plotted at mid width of the cavity and mid-height of the cavity respectively at different porosity. **Figure 7-A, B, C,** and **D** depicts *x*-components and *y*-components velocities for *AR* = 0.25 and 4.0 respectively at ε = 0.4, 0.6, and 0.9 for the case of no movement. **Figure 7-E, F, G,** and **H** depicts *x*-components and *y*-components velocities for *AR* = 0.25 and 4.0 respectively at ε = 0.4, 0.6, and 0.9 for the case of lower wall-driven. The effect of the moving wall is clear on the velocity distributions. The *y*-component velocity of flow is higher at the upper half of the cavity than that of bottom half. But for the *x*-component velocity is higher near the hot wall and it decreases continually with an increase in the horizontal distance.

Finally, **table 1** tabulated the average Nusselt number $\overline{Nu}$ for aspect ratio and movement effects. The conclusions from this table are:

1- The effect of wall movement in average Nusselt number is clear for all cases. The improvement is reach to 79 %.
2- The highest average Nusselt number is in case (78) for *AR* = 0.25 and ε = 0.9 with movement ($\overline{Nu} \approx 3.2$) (i.e. moving the big horizontal wall).
3- Cases (73, 74, and 75) are refused because they reduce the average Nusselt number compared with *AR* = 1.0 (i.e. horizontal position without movement at *AR* = 0.25 and ε = 0.4, 0.6, and 0.9).
4- The average Nusselt number increases as the porosity increases for the movement cases.
5- At the same porosity, as aspect ratio decreases the average Nusselt number decreases for no

movement cases. And at the same porosity, as aspect ratio decreases the average Nusselt number increases for movement cases.

REFERENCES

[1] Antonio F. MIGUEL, 2012, "Non-Darcy Porous Media Flow in No-Slip and Slip Regimes," THERMAL SCIENCE, vol. 16, 6, no. 1, pp. 167-176.

[2] Ayad F. Hameed, 2008, "Numerical Study of Free Convection Heat Transfer in a Cavity Filled With a Heat Generating Saturated Porous Medium," *Engineering and Technology Journal,* vol. 26, no. 4, pp. 169–187.

[3] C. Y. Wang, 2009, "The recirculating flow due to a moving lid on a cavity containing a Darcy–Brinkman medium," *A Applied Mathematical Modelling,* vol. *33,* pp. 2054–2061.

[4] Hakan F. Oztop, 2006, "Combined convection heat transfer in a porous lid-driven enclosure due to heater with finite length," *International Communications in Heat and Mass Transfer,* vol. *33,* pp. 772 – 779, March.

[5] Hakan F. Oztop, 2007, "Natural convection in partially cooled and inclined porous rectangular enclosures," I*nternational Journal of Thermal Sciences*, vol. 46, pp. 149–156, Elsevier.

[6] Laith J. Habeeb, 2012, "Numerical Simulation of Convective Heat Transfer and Fluid Flow through Porous Media with Different Moving and Heated Walls," Iraqi Journal for Mechanical and Materials Engineering, submitted for publication.

[7] M. A. Mohd Irwan, A. M. Fudhail, C. S. Nor Azwadi and G. Masoud, 2010, "Numerical Investigation of Incompressible Fluid Flow through Porous Media in a Lid-Driven Square Cavity," *American Journal of Applied Sciences,* vol. *7,* no. *10,* pp. 1341-1344.

[8] M. A. Waheed, G. A. Odewole and S. O. Alagbe, 2011, "Mixed Convective Heat Transfer In Rectangular Enclosures Filled With Porous Media," ARPN Journal of Engineering and Applied Sciences, vol. 6, no. 8, pp. 47-60, August.

[9] Mohamed A. Teamah and Wael M. El-Maghlany, 2010, "Numerical simulation of double-diffusive mixed convective fl ow in rectangular enclosure with insulated moving lid," *International Journal of Thermal Sciences,* vol. *49,* pp. 1625-1638.

[10] Mohd Irwan Bin Mohd Azmi, 2010, "Numerical Study of Convective Heat Transfer and Fluid Flow through Porous Media," *Master thesis,* University Technology Malaysia.

[11] Nithiarasu, P., Seetharamu, K. N. and Sundarajan, T., 1997, "Non-Darcy double-diffusive natural convectionin axisymmetric fluid saturated porous cavities," Heat and Mass Transfer, vol. 32, pp. 427-433, Springer-Verlag.

[12] Prakash Chandra and V. V. Satyamurty, 2011, "Non-Darcian and Anisotropic Effects on Free Convection in a Porous Enclosure," *Transp Porous Med,* vol. 90, pp. 301-320, May.

[13] Wenchao Liu, Jun Yao and Yueying Wang, 2012, "Exact analytical solutions of moving boundary problems of one-dimensional flow in semi-infinite long porous media with threshold pressure gradient," *International Journal of Heat and Mass Transfer*, vol. 55, pp. 6017–6022.

Table 1 Average Nusselt number for aspect ratio and movement effects.

AR	ε	U_{lid} = 0.0 m/s	U_{lid} = 0.2 m/s
0.25	0.4	0.7884136	1.311706
	0.6	0.7170379	1.785798
	0.9	0.6652881	3.217035
1.0	0.4	0.9989753	1.222328
	0.6	0.9958305	1.591573
	0.9	0.9915955	2.031172
4.0	0.4	1.011749	1.051095
	0.6	1.011716	1.069172
	0.9	1.011661	1.088600

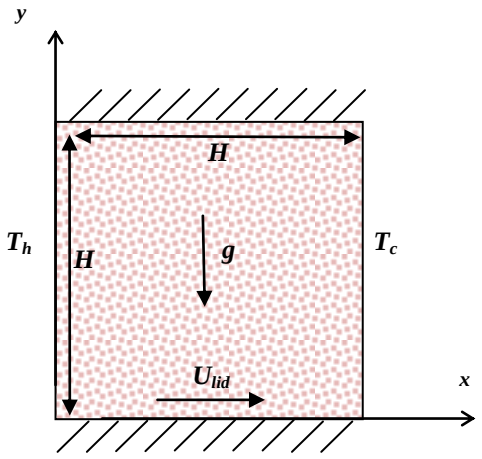

Figure 1 Schematic diagram for the physical model with the wall boundary constraints and the coordinate axes.

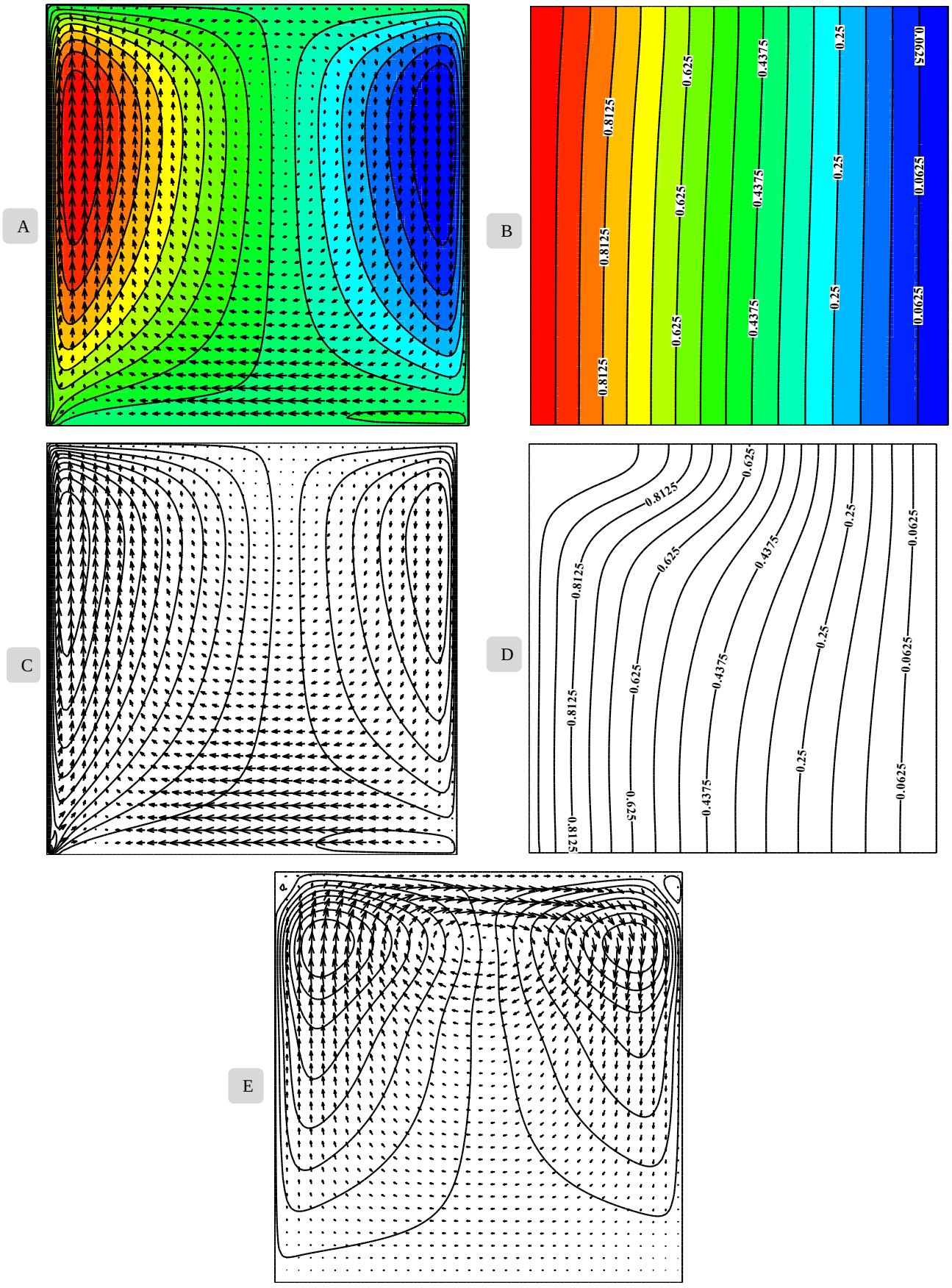

Figure 2 Velocity vectors, contours and temperature contours for stationary wall cavity at $Ra = 10^4$.

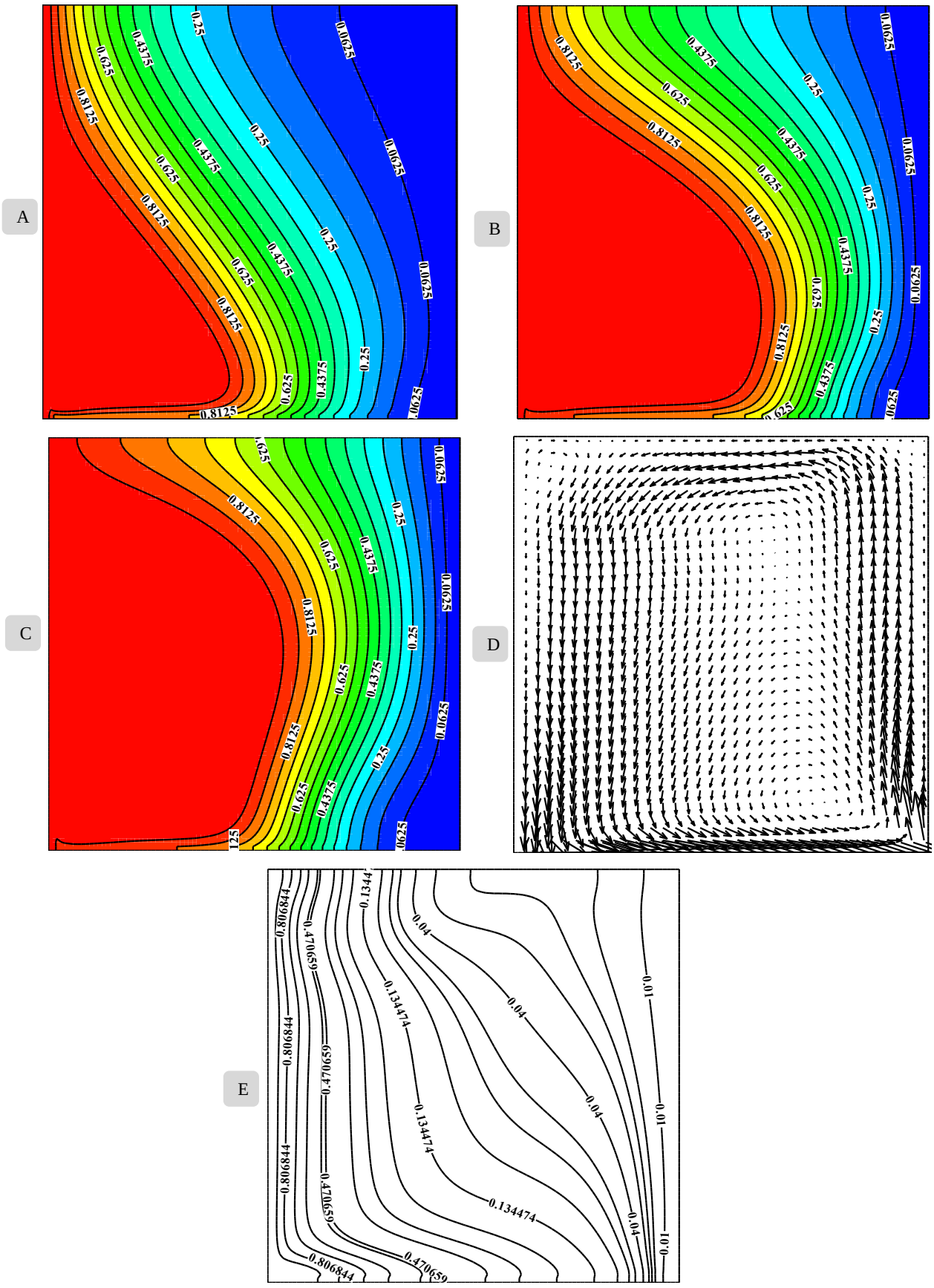

Figure 3 Temperature contours and velocity vectors for moving lower wall cavity at $Ra = 10^4$.

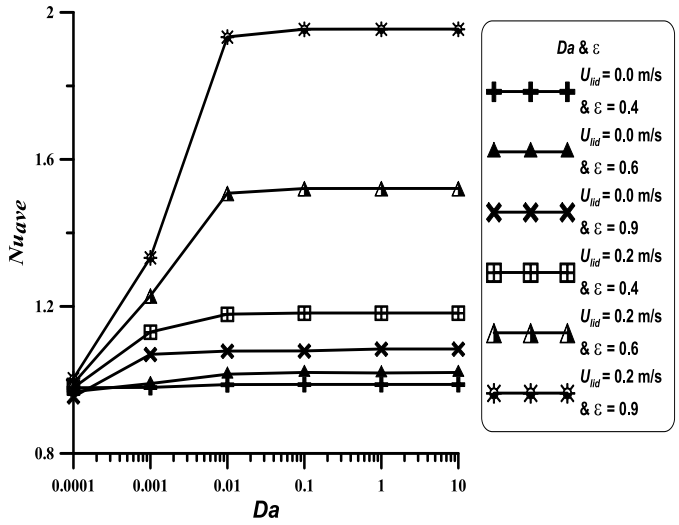

Figure 4 Average Nusselt number and Darcy number with and without movement.

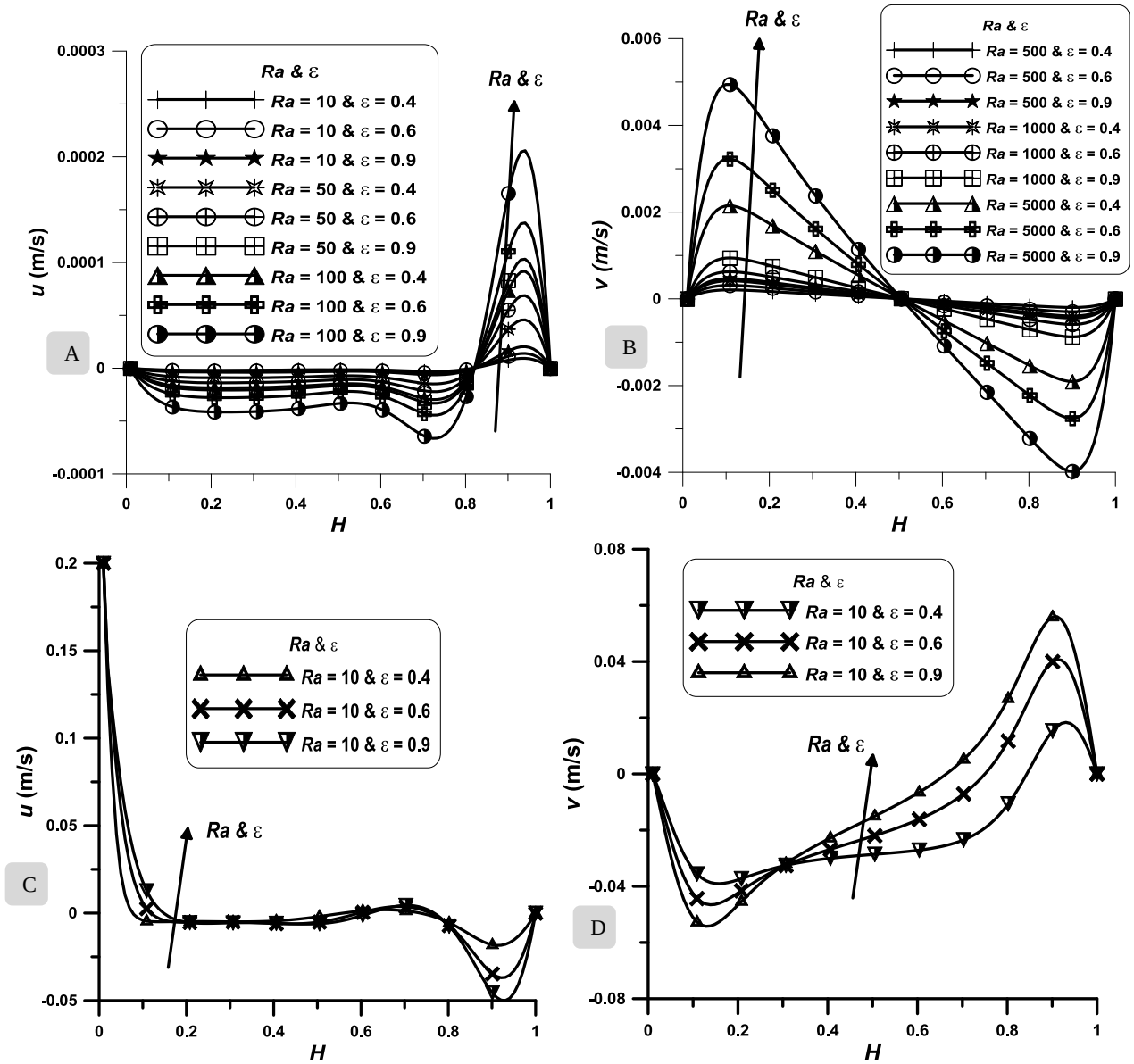

Figure 5 Velocities distributions at different *Ra* and *ε*.

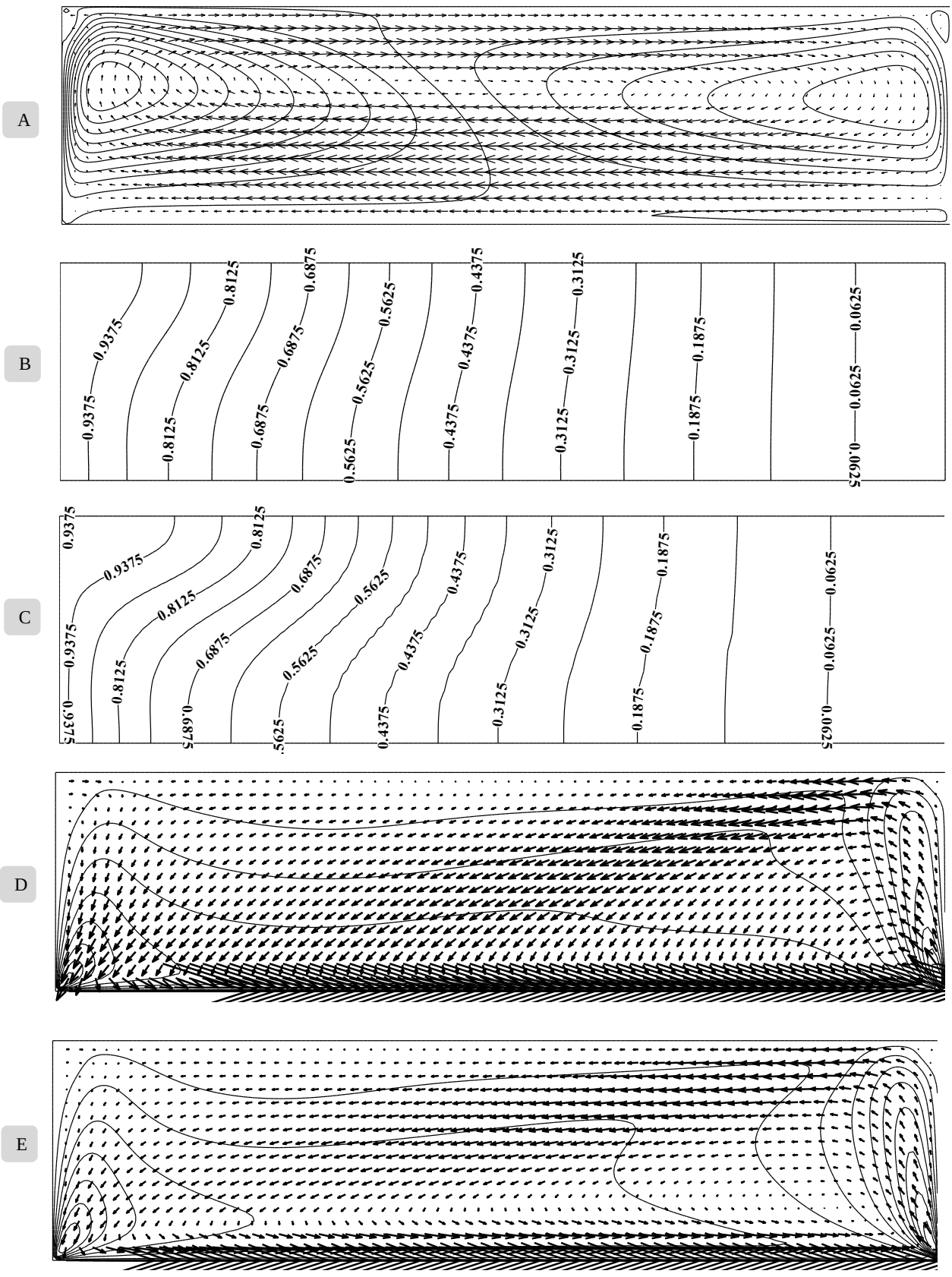
A
B
0.9375
0.8125
0.6875
0.5625
0.4375
0.3125
0.1875
0.0625
C
D
E

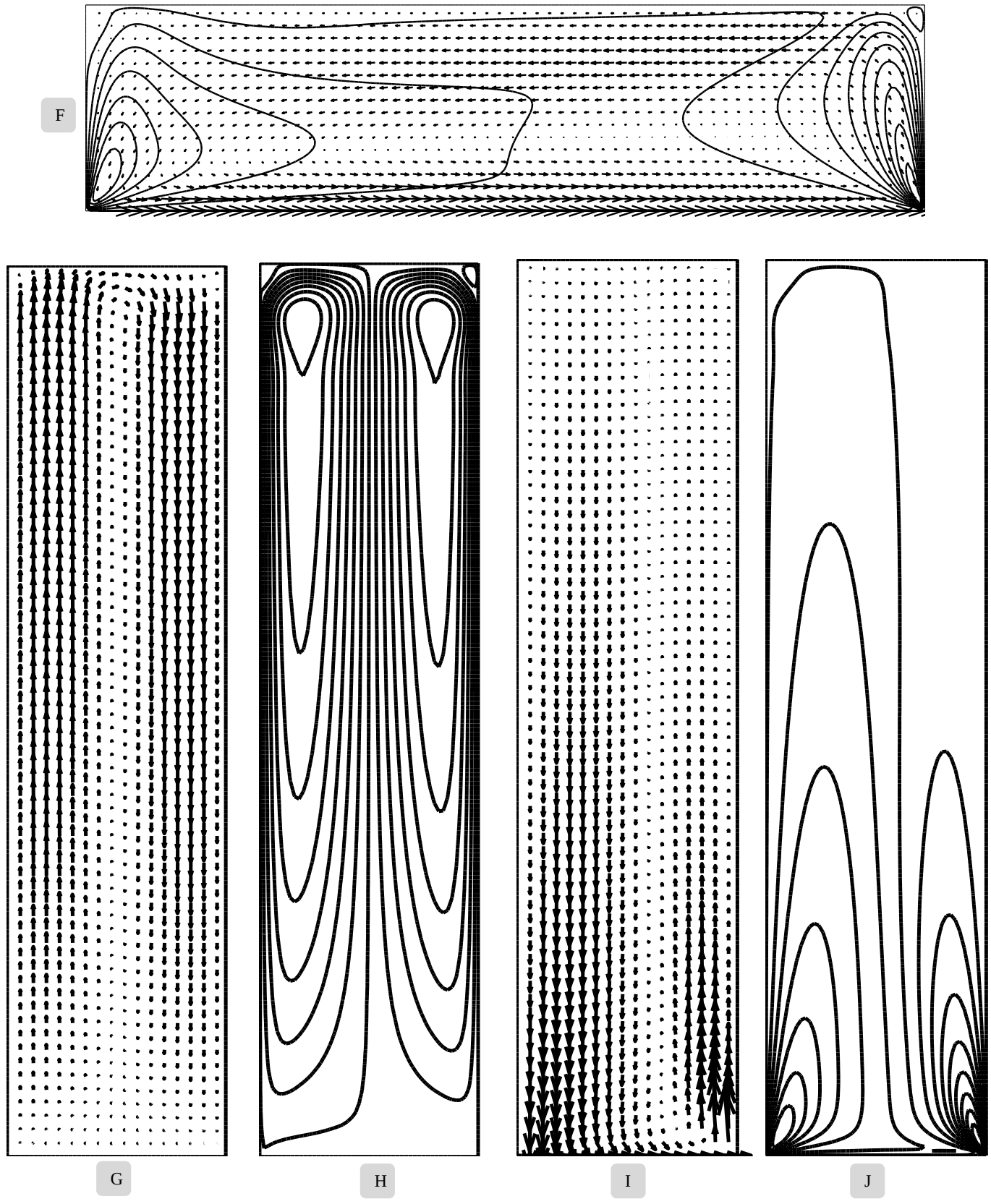

Figure 6 Velocities distributions at different *Ra* and ε.

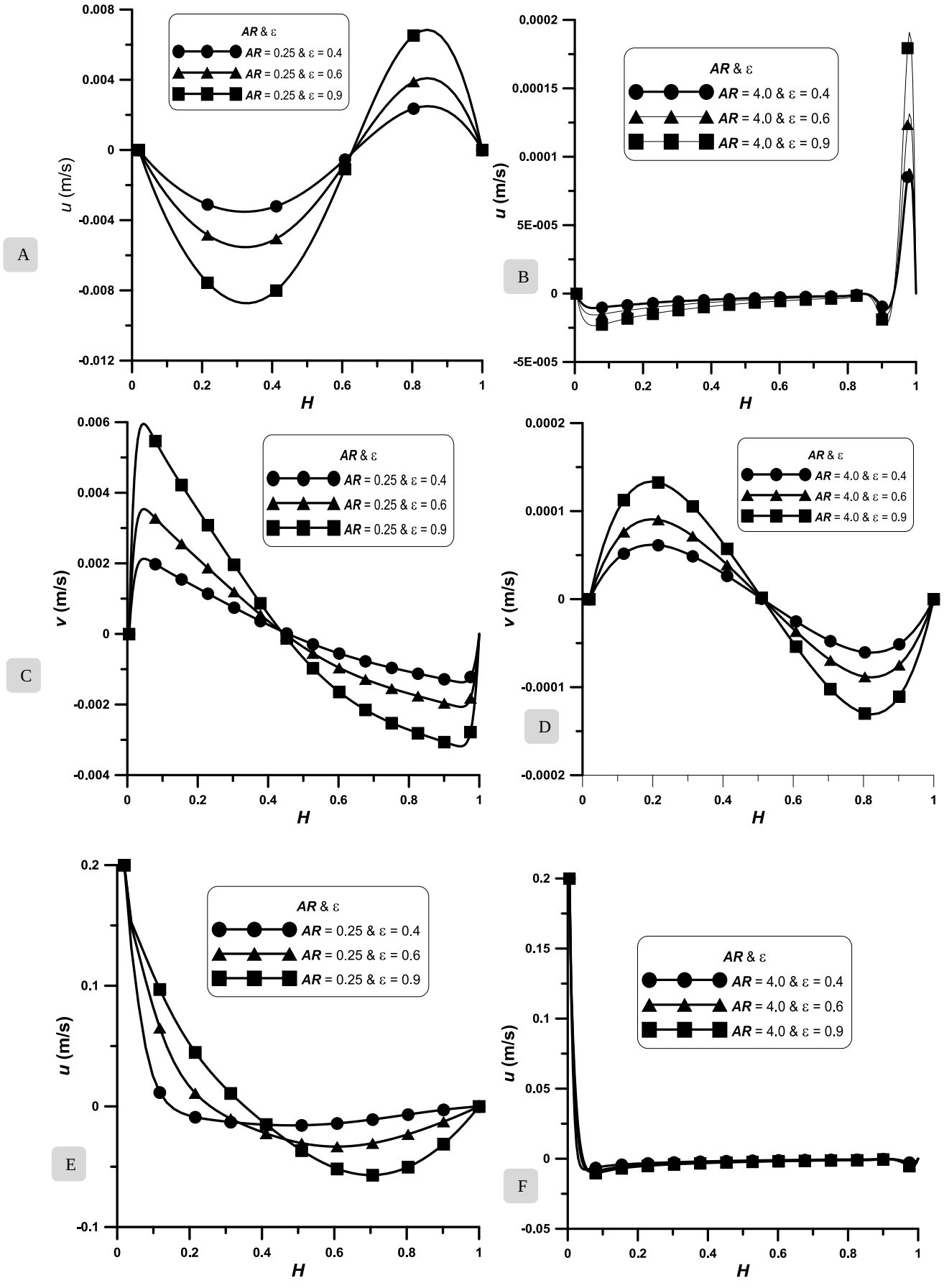
A
AR & ε
AR = 0.25 & ε = 0.4
AR = 0.25 & ε = 0.6
AR = 0.25 & ε = 0.9
u (m/s)
H
B
AR & ε
AR = 4.0 & ε = 0.4
AR = 4.0 & ε = 0.6
AR = 4.0 & ε = 0.9
u (m/s)
H
C
AR & ε
AR = 0.25 & ε = 0.4
AR = 0.25 & ε = 0.6
AR = 0.25 & ε = 0.9
v (m/s)
H
D
AR & ε
AR = 4.0 & ε = 0.4
AR = 4.0 & ε = 0.6
AR = 4.0 & ε = 0.9
v (m/s)
H
E
AR & ε
AR = 0.25 & ε = 0.4
AR = 0.25 & ε = 0.6
AR = 0.25 & ε = 0.9
u (m/s)
H
F
AR & ε
AR = 4.0 & ε = 0.4
AR = 4.0 & ε = 0.6
AR = 4.0 & ε = 0.9
u (m/s)
H

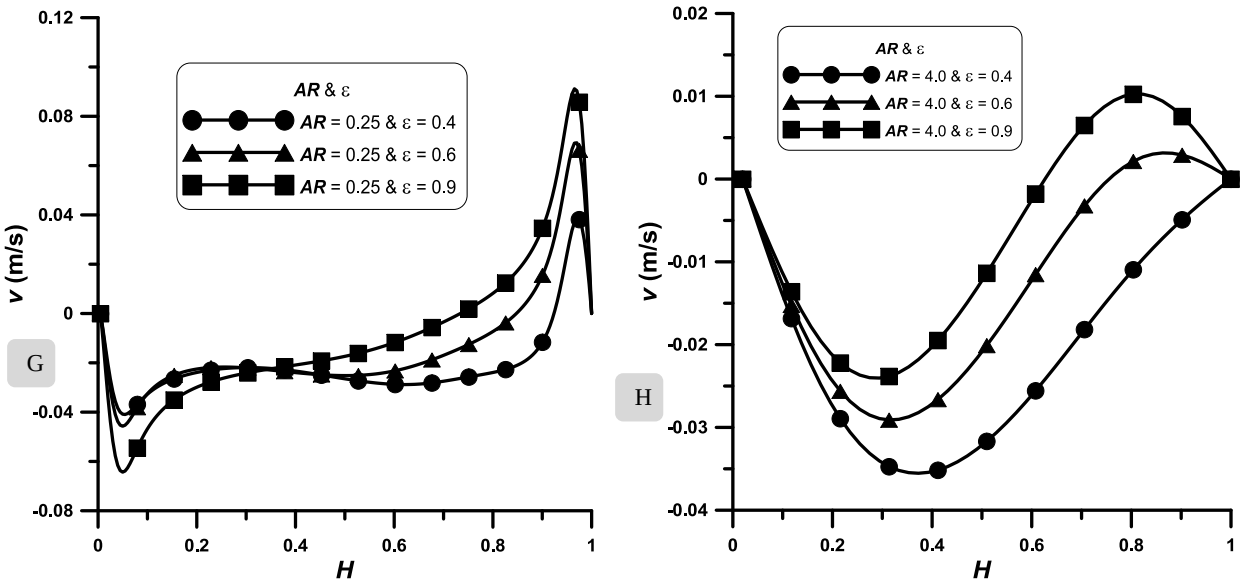

Figure 7 Velocities distributions at different *Ra* and *ε*.